Structural Engineering and Mechanics, Vol. 31, No. 6 (2009) 679-696
DOI: http://dx.doi.org/10.12989/sem.2009.31.6.679

Stresses around an underground opening with sharp corners due to non-symmetrical surface load

Karinski Y.S.†, Yankelevsky D.Z. and Antes M.Y.

National Building Research Institute, Faculty of Civil and Environmental Engineering, Technion - IIT, Haifa, 32000, Israel

(Received November 20, 2007, Accepted March 13, 2009)

Abstract. The paper aims at analyzing the stress distribution around an underground opening that is subjected to non-symmetrical surface loading with emphasis on opening shapes with sharp corners and the stress concentrations developed at these locations. The analysis is performed utilizing the BIE method coupled with the Neumann's series. In order to implement this approach, the special recurrent relations for half plane were proven and the modified Shanks transform was incorporated to accelerate the series convergence. To demonstrate the capability of the developed approach, a horseshoe shape opening with sharp corners was investigated and the location and magnitude of the maximum hoop stress was calculated. The dependence of the maximum hoop stress location on the parameters of the surface loading (degree of asymmetry, size of loaded area) and of the opening (the opening height) was studied. It was found that the absolute magnitude of the maximum hoop stress (for all possible surface loading locations) is developed at the roof points when the opening height/width ratio is relatively large or when the pressure loading area is relatively narrow (compared to the roof arch radius), and contrarily, when the opening height/width ratio is relatively small or when the surface pressure is applied to a relatively wide area, the absolute magnitude of the maximum hoop stress is developed at the bottom sharp corner points.

Keywords: boundary element method; buried structures; half space; openings; stress concentration.

1. Introduction

Shallow tunnels in soil are commonly used for different purposes such as utility conduits, transportation tunnels etc. Shallow tunnels with a limited soil cover depth from ground surface are sensitive the surface loading (Szechny 1973, Fernando *et al.* 1996, Fernando and Carter 1998, Guzina *et al.* 2003). Commonly a symmetrical surface loading is considered in the stress analysis of an underground opening, mainly for simplicity, however a non-symmetrical loading may yield extreme stress conditions around the opening (Moser 2001, Hatzor *et al.* 2002).

When the opening (cavity) has a circular shape, the analysis can be carried out using analytical or semi-analytical solution techniques (Moore 1987, Karinski *et al.* 2003), that are based on the application of Fourier series (Small and Wang 1988) or Fourier-Bessel series (Karinski *et al.* 2004, 2007), as well as of using the Muskhelishvili's method complex variables theory (Chen 1994). For other cavity shapes numerical methods are applied. The most widely employed numerical technique

† Ph.D., Corresponding author, E-mail: karinski@technion.ac.il

is the finite element method (FEM) (Kumar 1985, Dajapakse and Senjuntichi 1995, Moore and Branchman (1994). When the soil medium may be considered linear, the boundary integral equation method (BIEM) (Brebbia and Walker 1980, Talles 1983, Antonio and Tadeu 2002, Manolis 2003) may be applied, and when the entire medium is linear and only the near field is not linear, the coupled FEM-BIEM method (Kim *et al.* 2000, Surjadinata *et al.* 2006, Andersen and Jones 2006) may be used.

Commonly standard nodal collocation schemes are utilized in applications of the BIEM that lead to a linear algebraic system of equations (Brebbia and Walker 1980, Cruse 1973, Cavalcanti and Telles 2003). Another approach to solve the boundary integral equations is to apply the Neumann-type series (Hurty and Rubinstein 1964, Karal and Keller 1964) that avoids the need to solve a large system of equations with a densely populated matrix of non zero terms. Perlin (1984) proved that the Fredholm alternatives are valid for the integral equations with the singular kernel of Kelvin-Somiliagna type that are typical for elastostatics. Therefore, the solution of such equations may also be represented in the form of Neumann's series. This approach includes a regular representation of singular integrals and is using some special recurrent relationships, which were obtained for a both internal (relating to a bounded finite medium) and external (Antes *et al.* 2007) (relating to an infinite medium includes cavities) problems.

The convergence of the Neumann's series depends on the boundary curvature and its differential properties, but some special methods (Kantorovich 1958) may efficiently accelerate this convergence. One of these methods is the Shanks transform (Shanks 1955, Antes *et al.* 2007) which is widely used in the solution of electrodynamics integral equations (Rogier-Hendrik and De-Zutter 2002) but has not yet been implemented in elestostatics and elastodynamics problems.

The present paper aims at developing the implementation of the BIE method coupled with the Neumann's series for the analysis of the buried opening in soil, with emphasis on opening contours having sharp corners that lead to hoop stress concentrations. The case of a non symmetrical surface loading is considered, as it may yield higher stresses compared to the case of symmetrical surface loading, and thus determine a critical state of stress around the opening. To accelerate the series convergence the modified Shanks transform is proposed.

2. Basic relationships

Consider the second boundary problem (where boundary stresses are given) for a half plane which occupies a domain D^- with a boundary S (see Fig. 1).

If a force $\boldsymbol{T}_\nu = \{T_1(\boldsymbol{q}), T_2(\boldsymbol{q})\}$ is applied at a given point $\boldsymbol{q} = \{y_1, y_2\}$ of the boundary S, the integral equation for the displacement $\mathbf{u} = \{u_1, u_2\}$ at a certain point of the domain $\boldsymbol{p} = \{x_1, x_2\}$ is given in the following form

$$
\begin{aligned}
2\mathbf{u}(\mathbf{p}) &= -\int_S \Gamma_2(\mathbf{p},\mathbf{q})\mathbf{u}(\mathbf{q})dS_q - \int_S \Gamma(\mathbf{p},\mathbf{q})\mathbf{T}_\nu(\mathbf{q})dS_q, \quad \mathbf{p} \in D^- \\
0 &= \int_S \Gamma_2(\mathbf{p},\mathbf{q})\mathbf{u}(\mathbf{q})dS_q - \int_S \Gamma(\mathbf{p},\mathbf{q})\mathbf{T}_\nu(\mathbf{q})dS_q, \quad \mathbf{p} \in D^+
\end{aligned} \tag{1}
$$

Where $\Gamma_2(\mathbf{p}, \mathbf{q})$ and $\Gamma(\mathbf{p}, \mathbf{q})$ are the stress operator and the Green function respectively.

For a half plane, these functions consist of two parts: the singular term (marked by the index "k") which is the corresponding function for the plane and the additional regular term (marked by the index "c") (Talles 1983, Melan 1932)

$$\Gamma_2(\mathbf{p},\mathbf{q}) = \Gamma_2^K(\mathbf{p},\mathbf{q}) + \Gamma_2^c(\mathbf{p},\mathbf{q});$$
$$\Gamma(\mathbf{p},\mathbf{q}) = \Gamma^K(\mathbf{p},\mathbf{q}) + \Gamma^c(\mathbf{p},\mathbf{q}) \tag{2}$$

For a two-dimensional problem, the singular terms are the following

$$\Gamma_{ij}^K(\mathbf{p},\mathbf{q}) = \frac{1}{2\pi\mu(\lambda+2\mu)}\left[(\lambda+\mu)\frac{\partial\mathbf{r}}{\partial x_i}\frac{\partial\mathbf{r}}{\partial x_j} + (\lambda+3\mu)\delta_{ij}\ln\frac{1}{\mathbf{r}(\mathbf{p},\mathbf{q})}\right] \tag{3}$$

$$\Gamma_{2ij}^K(\mathbf{p},\mathbf{q}) = \frac{1}{2}\left[m\,\delta_{ij} + \frac{2}{3}n\frac{(y_i-x_i)(y_j-x_j)}{\mathbf{r}^2}\right]\sum_{l=1}^{3}\frac{(y_l-x_l)v_l(\mathbf{q})}{\mathbf{r}^2} +$$
$$+\frac{m}{2}\left[v_i(\mathbf{q})\frac{(y_j-x_j)}{\mathbf{r}^2} - v_j(\mathbf{q})\frac{(y_i-x_i)}{\mathbf{r}^2}\right] \tag{4}$$

The additional terms (Talles 1983) for the Green function $\Gamma^c = \{2u_{ij}^c\}$ and for the stress operator $\Gamma_2^c = \{\Gamma_{2ij}^C\} = \left\{2\sum_k \sigma_{jki}^C \mathbf{v}_k\right\}$, which do not contain the singularities, are presented in Appendix A.

3. Solution of the basic Eq. (1) by Neumann series

Consider the problem in which the displacements function satisfies the Hölder-Lipschitz condition of order 1

$$\sup_{q,q' \in S} \|\mathbf{u}(\mathbf{p}) - \mathbf{u}(\mathbf{q})\| \le A\|\mathbf{p}-\mathbf{q}\|; \quad A > 0 \tag{5}$$

The solution of the displacements function is presented in the form of Neumann's series by powers of the parameter λ as follows

$$\mathbf{u}(\mathbf{q}) = \sum_{n=0}^{\infty}\lambda^n \mathbf{u}_n(\mathbf{q}) \tag{6}$$

Substitution of Eq. (6) into Eq. (1) and further equating coefficients of equal powers of λ, leads to the following recurrent relationships

$$\mathbf{u}_n(\mathbf{p}) = \int_S \Gamma_2(\mathbf{p},\mathbf{q})\mathbf{u}_{n-1}(\mathbf{q})dS_q;$$
$$\left(n = 1,2,\ldots;\ \mathbf{u}_0(\mathbf{q}) = -\int_S \Gamma(\mathbf{q},\mathbf{q}')\mathbf{T}_\nu(\mathbf{q}')dS_{q'}\right) \tag{7}$$

The integral term in Eq. (7) is singular; therefore it can't be calculated by using any quadrature formula. The regularization is performed by a procedure that had been suggested by Perlin (Parton and Perlin 1984, Kantorovich 1958).

Define a constant vector $\boldsymbol{u}_0$ in the domain $D^{-}\cup S$ (Fig. 1). The vector represents a rigid body displacement of the entire domain D^{-}. Therefore Eq. (1) yield

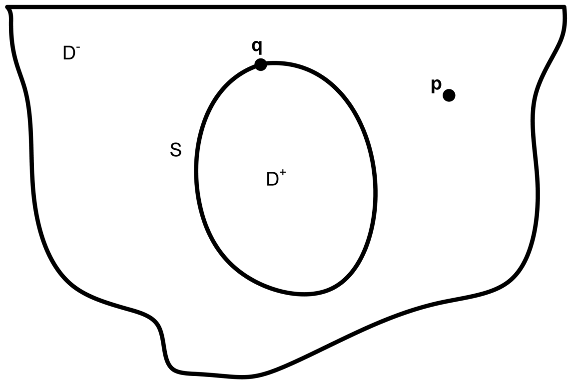

Fig. 1 The problem domain

$$\int_S \boldsymbol{\Gamma}_2(\mathbf{p},\mathbf{q})\mathbf{u}_0 dS_q = 0\,, \quad \mathbf{p} \in D^+$$
$$2\mathbf{u}_0 = \int_S \boldsymbol{\Gamma}_2(\mathbf{p},\mathbf{q})\mathbf{U}_0 dS_q = 0\,, \quad \mathbf{p} \in D^- \tag{8}$$

Hence the following relationships for the stress function are

$$\int_S \boldsymbol{\Gamma}_2(\mathbf{p}_1,\mathbf{q}) dS_q = 0, \quad \mathbf{p} \in D^+ \tag{9}$$

$$\int_S \boldsymbol{\Gamma}_2(\mathbf{p}_1,\mathbf{q}) dS_q = 2\mathbf{E}, \quad \mathbf{p} \in D^- \tag{10}$$

The corresponding relationship on the boundary S is found from Eqs. (9-10) due to the well known procedure of the determination of the boundary value of a function (Brebbia and Walker 1980) as follows

$$\int_S \boldsymbol{\Gamma}_2(\mathbf{q}_1,\mathbf{q}) dS_q = \mathbf{E}, \quad \mathbf{q}_1 \in S \tag{11}$$

Multiplying Eq. (11) by the constant vector $\mathbf{u}(\mathbf{q}_1)$ yields

$$\mathbf{u}(\mathbf{q}_1)\Big(\mathbf{E} - \int_S \boldsymbol{\Gamma}_2(\mathbf{q}_1,\mathbf{q}) dS_q\Big) = 0 \tag{12}$$

where $\mathbf{E}$ is the identity 2×2 matrix.

Adding the integral $\int_S \boldsymbol{\Gamma}_2(\mathbf{q}_1,\mathbf{q})\mathbf{u}(\mathbf{q}) dS_q$ to the left-hand side and to the right-hand side of Eq. (12) one obtains the following identity

$$\int_S \boldsymbol{\Gamma}_2(\mathbf{q}_1,\mathbf{q})\mathbf{u}(\mathbf{q}) dS_q = \mathbf{u}(\mathbf{q}_1) + \int_S \boldsymbol{\Gamma}_2(\mathbf{q}_1,\mathbf{q})[\mathbf{u}(\mathbf{q}) - \mathbf{u}(\mathbf{q}_1)] dS_q \tag{13}$$

For the half plane the stress operator is given as a sum (2) and therefore Eq. (13) takes the following form

$$\int_S [\Gamma_2^k(\mathbf{q}_1,\mathbf{q}) + \Gamma_2^c(\mathbf{q}_1,\mathbf{q})]\mathbf{u}(\mathbf{q})dS_q = \mathbf{u}(\mathbf{q}_1) + \int_S [\Gamma_2^k(\mathbf{q}_1,\mathbf{q}) + \Gamma_2^c(\mathbf{q}_1,\mathbf{q})][\mathbf{u}(\mathbf{q}) - \mathbf{u}(\mathbf{q}_1)]dS_q \tag{14}$$

The additional part Γ_2^c of the stress operator is regular and the following condition is valid

$$\int_S \Gamma_2^c(\mathbf{q}_1,\mathbf{q})[\mathbf{u}(\mathbf{q}) - \mathbf{u}(\mathbf{q}_1)]dS_q = 0 \tag{15}$$

Therefore, the identity in Eq. (14) becomes

$$\int_S \Gamma_2^k(\mathbf{q}_1,\mathbf{q})\mathbf{u}(\mathbf{q})dS_q = \mathbf{u}(\mathbf{q}_1) + \int_S \Gamma_2^k(\mathbf{q}_1,\mathbf{q})[\mathbf{u}(\mathbf{q}) - \mathbf{u}(\mathbf{q}_1)]dS_q - \int_S \Gamma_2^c(\mathbf{q}_1,\mathbf{q})\mathbf{u}(\mathbf{q})dS_q \tag{16}$$

Substitution of Eq. (16) into the recurrent expression (7) yields the following recurrent relationship

$$\mathbf{u}_n(\mathbf{p}) = \mathbf{u}_{n-1}(\mathbf{p}) + \int_S \Gamma_2^k(\mathbf{p},\mathbf{q})[\mathbf{u}_{n-1}(\mathbf{q}) - \mathbf{u}_{n-1}(\mathbf{p})]dS_q - \int_S \Gamma_2^c(\mathbf{p},\mathbf{q})\mathbf{u}_{n-1}(q)dS_q \tag{17}$$

Hereafter it is assumed that the boundary "*S*" (see Fig. 1) does not intersect with the half plane boundary at the source point (i.e., $c \neq 0$ in Fig. 16). Therefore as it was already mentioned earlier, the additional part of the stress operator Γ_2^c is regular, and therefore the second integral of the right-hand side of Eq. (17) is regular as well.

On the other hand, the singular part of the stress operator Γ_2^K has a singularity of the order of $1/r$, the displacements function satisfies condition (7), and the first integral of the right-hand side of Eq. (17) is also regular. The relationship (17) is the regular form of the base recurrent formulas (7) and can be calculated by any known quadrature rule.

4. Modified Shanks Transform

As was already mentioned earlier, the solution of the boundary integral Eq. (1) may be presented in the form of Neumann's series (6). Its convergence depends on the boundary form, on its curvature, on the differential properties and the presence of corner points (Parton and Perlin 1984, Mikhlin 1965, Schnack and Tuerke 1997).

To accelerate the solution convergence, the following Shanks transform (Shanks 1955) of the partial sum $S_n = \sum_{j=0}^{n} \lambda^j \varphi_j(q)$ $(n = k, k+1, k+2, \ldots)$ may by applied

$$\sigma_{kn} = \frac{D_{kn}(S_n)}{D_{kn}} \tag{18}$$

Here

$$D_{kn} = \begin{vmatrix} 1 & 1 & \ldots & 1 \\ \Delta S_{n-k} & \Delta S_{n-k+1} & \ldots & \Delta S_n \\ \Delta S_{n-k+1} & \Delta S_{n-k+2} & \ldots & \Delta S_{n+1} \\ \ldots & \ldots & \ldots & \ldots \\ \Delta S_{n-1} & \Delta S_n & \ldots & \Delta S_{n+k-1} \end{vmatrix} \tag{19}$$

$$D_{kn}(S_n) = \begin{vmatrix} S_{n-k} & S_{n-k+1} & \cdots & S_n \\ \Delta S_{n-k} & \Delta S_{n-k+1} & \cdots & \Delta S_n \\ \Delta S_{n-k+1} & \Delta S_{n-k+2} & \cdots & \Delta S_{n+1} \\ \cdots & \cdots & \cdots & \cdots \\ \Delta S_{n-1} & \Delta S_n & \cdots & \Delta S_{n+k-1} \end{vmatrix} \tag{20}$$

$\Delta S_n = S_{n+1} - S_n$; $1 \le k \le n-1$ is the order of the Shanks transform.

This transform exists in the case of $D_{kn} \neq 0$ only. But in that approach one needs to evaluate the differences ΔS_n and the above determinants at any step of calculation. To avoid such inconveniences the following modified Shanks transform (Antes *et al.* 2007) is suggested.

Let's add together the previous and the following rows of the determinant (20) beginning from the first row (and placing the result into the "following" row). Therefore Eq. (20) takes the form

$$D_{kn}(S_n) = \begin{vmatrix} S_{n-k} & S_{n-k+1} & \cdots & S_n \\ S_{n-k+1} & S_{n-k+2} & \cdots & S_{n+1} \\ S_{n-k+2} & S_{n-k+3} & \cdots & S_{n+2} \\ \cdots & \cdots & \cdots & \cdots \\ S_n & S_{n+1} & \cdots & S_{n+k} \end{vmatrix} \tag{21}$$

Expanding Eq. (19) for all ΔS_j ($j = n - k, n - k + 1, \ldots n + k - 1$), reducing corresponding terms and changing the unit row position according to the term number, one obtains the following determinants sum

$$D_{kn} = \begin{vmatrix} 1 & 1 & \cdots & 1 \\ S_{n-k+1} & S_{n-k+2} & \cdots & S_{n+1} \\ S_{n-k+2} & S_{n-k+3} & \cdots & S_{n+2} \\ \cdots & \cdots & \cdots & \cdots \\ S_n & S_{n+1} & \cdots & S_{n+k} \end{vmatrix} + \begin{vmatrix} S_{n-k} & S_{n-k+1} & \cdots & S_n \\ 1 & 1 & \cdots & 1 \\ S_{n-k+2} & S_{n-k+3} & \cdots & S_{n+2} \\ \cdots & \cdots & \cdots & \cdots \\ S_n & S_{n+1} & \cdots & S_{n+k} \end{vmatrix}$$

$$+ \ldots + \begin{vmatrix} S_{n-k} & S_{n-k+1} & \cdots & S_n \\ S_{n-k+1} & S_{n-k+2} & \cdots & S_{n+1} \\ S_{n-k+2} & S_{n-k+3} & \cdots & S_{n+2} \\ \cdots & \cdots & \cdots & \cdots \\ 1 & 1 & \cdots & 1 \end{vmatrix} \tag{22}$$

Substitution of Eqs. (21), (22) into Shanks transform (18) and division of the numerator and denominator by the non-zero determinant (21) yields the expression for σ_{kn} in the form

$$\sigma_{kn} = \frac{1}{\sum_{j=1}^{k+1} \zeta_j} \tag{23}$$

Where ζ_j ($j = 1, 2, \ldots, k + 1$) are the solutions of the following system of equations

$$\begin{bmatrix} S_{n-k} & S_{n-k+1} & \cdots & S_n \\ S_{n-k+1} & S_{n-k+2} & \cdots & S_{n+1} \\ S_{n-k+2} & S_{n-k+3} & \cdots & S_{n+2} \\ \cdots & \cdots & \cdots & \cdots \\ S_n & S_{n+1} & \cdots & S_{n+k} \end{bmatrix} \begin{bmatrix} \zeta_1 \\ \zeta_2 \\ \zeta_3 \\ \cdots \\ \zeta_{k+1} \end{bmatrix} = \begin{bmatrix} 1 \\ 1 \\ 1 \\ \cdots \\ 1 \end{bmatrix} \tag{24}$$

Therefore, applying this type of Shanks transform enables the solution of the system of n linear algebraic equations, with a relatively limited number of iterations n.

5. Consideration of the surface load

When a part of the half plane surface S_2 (Fig. 2) is loaded, this loaded segment must be included in the boundary S for which the integration is performed. Therefore Eq. (1) is obtained in the following form

$$\begin{aligned} 2\mathbf{u}(\mathbf{p}) &= -\int_{S_1 \cup S_2} \Gamma_2(\mathbf{p},\mathbf{q})\mathbf{u}(\mathbf{q})dS_q - \int_{S_1 \cup S_2} \Gamma(\mathbf{p},\mathbf{q})\mathbf{T}_\nu(\mathbf{q})dS_q, \quad \mathbf{p} \in D^- \\ 0 &= \int_{S_1 \cup S_2} \Gamma_2(\mathbf{p},\mathbf{q})\mathbf{u}(\mathbf{q})dS_q - \int_{S_1 \cup S_2} \Gamma(\mathbf{p},\mathbf{q})\mathbf{T}_\nu(\mathbf{q})dS_q, \quad \mathbf{p} \in D^+ \end{aligned} \tag{25}$$

Where S_1 is the cavity boundary, $S = S_1 U S_2$.

The integral kernels are presented as a sum of singular and regular parts (see (2)). For the regular parts (see Appendix A) the mentioned above integrals may be represented as a sum by S_1 and S_2 for any type of the boundary. For the singular integrals it is possible under the following theorem (Kupradze *et al.* 1979) conditions:

For any multicell domain $S = \bigcup_{i=1}^{N} S_i$, such as $\bigcap_{i=1}^{N} S_i = \varnothing$, for each $k \neq m$ $(1 \le k \le N;\ 1 \le m \le N)$ the

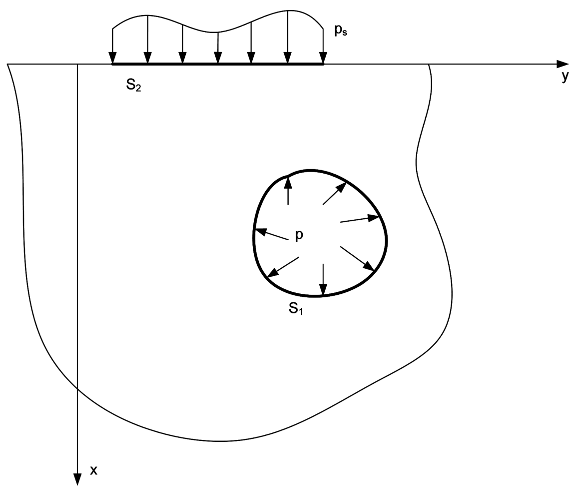

Fig. 2 The surface load

singular integrals with the kernel of the type $1/r$ have a property of additibility by the measure.

As it was already mentioned earlier, it is assumed that the boundary "S_1" (see Fig. 2) does not intersect with the half plane boundary $S_1 \cap S_2 = \varnothing$. Furthermore the integral kernels have a form (3,4). Therefore all the singular integrals of Eq. (25) are under the conditions of the Kupradze's theorem (Kupradze *et al.* 1979) and may be represented as a sum by S_1 and S_2 separately. Therefore the recurrent relationships (17) take the following form

$$\begin{aligned}\mathbf{u}_n(\mathbf{p}) = \mathbf{u}_{n-1}(\mathbf{p}) + \int_{S_1}\Gamma_2^k(\mathbf{p},\mathbf{q})[\mathbf{u}_{n-1}(\mathbf{q}) - \mathbf{u}_{n-1}(\mathbf{p})]dS_q - \int_{S_1}\Gamma_2^c(\mathbf{p},\mathbf{q})\mathbf{u}_{n-1}(q)dS_q + \\ + \int_{S_2}\Gamma_2^k(\mathbf{p},\mathbf{q})[\mathbf{u}_{n-1}(\mathbf{q}) - \mathbf{u}_{n-1}(\mathbf{p})]dS_q - \int_{S_2}\Gamma_2^c(\mathbf{p},\mathbf{q})\mathbf{u}_{n-1}(q)dS_q\end{aligned} \tag{26}$$

Note that the part S_2 of the half plane is finite, and therefore the usage of the Green's tensor for the half plane enables to avoid integration over the infinite domain.

6. Analysis of a circular cavity

To compare the results obtained by the present approach (Neumann's series and Shanks transform) with known results, analysis will be carried out for a circular cavity of a radius r_0 that is buried in a half-plane at depth H below the surface. The stress distribution around the opening will be calculated for the following data: top surface is loaded by a symmetrical load p_s (see Fig. 3) uniformly distributed along a segment of width $2L$. Young's modulus E = 30 MPa and Poisson ratio $\nu = 0.46$. The comparison of the calculated results with the proposed model (hoop stress $\sigma_{\theta\theta}$ normalized with respect to the surface pressure p_s) with the closed form solution presented by Bulichov (1989) shows good agreement (see Table 1). The analysis was carried out using a 96 linear elements subdivision of the cavity perimeter and 200 elements on the loaded part of the half plane surface. For the circular cavity only 15 iterations (26) were needed to achieve this accuracy.

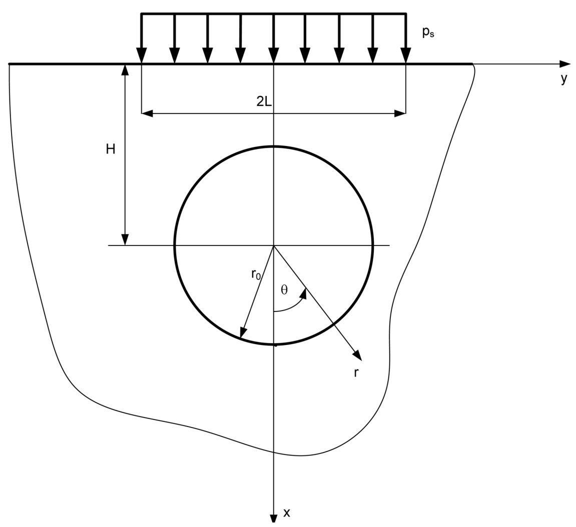

Fig. 3

Table 1

θ^0	$H/r_0 = 1.25$						$H/r_0 = 2$					
	$L/r_0 = 0.31$		$L/r_0 = 1.25$		$L/r_0 = 10$		$L/r_0 = 0.5$		$L/r_0 = 2.0$		$L/r_0=16$	
	Test	BIE	Test	BIE	Test	BIE	Test	BIE	Test	BIE	Test	BIE
0	−0.21	−0.21	−0.39	−0.39	1.23	1.24	−0.17	−0.17	−0.31	−0.31	1.35	1.35
15	−0.19	−0.19	−0.31	−0.30	1.34	1.35	−0.14	−0.14	−0.21	−0.20	1.43	1.44
30	−0.13	−0.12	−0.05	−0.04	1.62	1.64	−0.05	−0.05	0.12	0.12	1.65	1.66
45	−0.00	−0.00	0.38	0.39	2.02	2.05	0.10	0.10	0.62	0.63	1.95	1.96
60	0.17	0.17	1.01	1.01	2.50	2.51	0.31	0.31	1.28	1.28	2.26	2.27
75	0.42	0.42	1.84	1.85	2.97	2.98	0.56	0.56	1.99	1.99	2.52	2.53
90	0.79	0.79	2.91	2.92	3.46	3.48	0.95	0.84	2.65	2.65	2.69	2.70
105	1.33	1.31	4.19	4.20	4.05	4.07	1.13	1.12	3.03	3.03	2.75	2.76
120	2.13	2.10	5.41	5.42	4.77	4.79	1.32	1.30	2.91	2.92	2.70	2.70
135	3.20	3.14	5.89	5.90	5.43	5.46	1.24	1.23	2.18	2.18	2.50	2.50
150	3.73	3.65	4.85	4.85	5.30	5.32	0.64	0.64	1.03	1.03	2.14	2.15
165	0.51	0.54	1.21	1.23	3.30	3.32	−0.41	−0.40	−0.06	−0.06	1.76	1.77
180	−3.60	−3.50	−1.80	−1.76	1.44	1.47	−1.00	−0.99	−0.52	−0.52	1.58	1.59

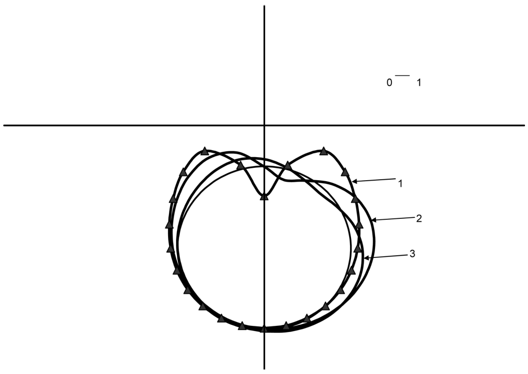

Fig. 4 Hoop stress distribution for circular cavity: 1 – $\Delta/r_0 = 0$, symmetrical loading (▲ the test solution, ▬ - present solution); 2 – $\Delta/r_0 = 1$; 3 – $\Delta/r_0 = 2$

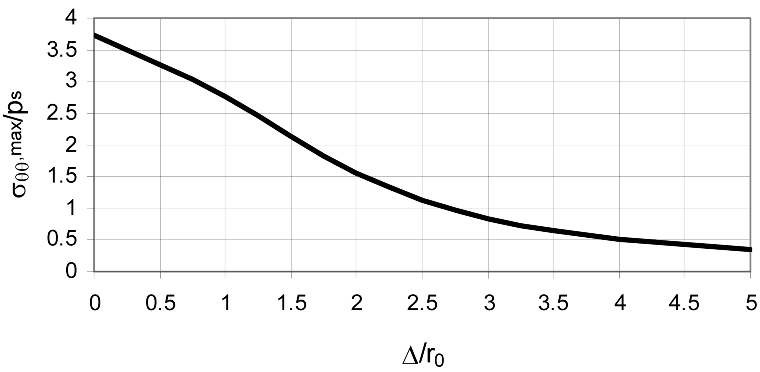

Fig. 5 Maximum hoop stress for the circle cavity subjected by the non-symmetrical surface load

The maximum error was obtain in the case of $L/r_0 = 0.31$, H/r_0=1.25 (θ = 180°) and was found to be less than 3%. The stress distribution for this case is shown in Fig. 4 (line 1: triangles – closed form solution, solid line – present solution).

In the case of nonsymmetrical loading the location of the maximum stress is shifted (smaller angle θ defines the location of the maximum stress for a resultant external force acting right to the geometrical axis of symmetry) and its magnitude decreases as shown in Fig. 5. Here Δ is the distance between the load resultant location and the geometrical axis of symmetry. Examples of the stress distributions for different non-symmetrical loadings are shown in the Fig. 4 (lines 2 and 3).

7. Analysis of a horseshoe cavity

When the cavity has sharp corner points where stress concentration may develop, the dependence of the maximum hoop stress on the non-symmetrical surface load has a different nature. It may be demonstrated in the examination of a horseshoe cavity (with an arch radius R and walls height A) that is located in an elastic medium ($E = 30$ MPa, $\nu = 0.25$). A non-symmetrical uniformly distributed load with intensity p_s is applied to a segment of width $2L$ (see Fig. 6). The arch centre depth is $H = 1.25R$ and the distance of the load resultant from the arch centre is denoted as Δ. The calculations were performed with linear boundary elements: 8 elements along every wall and alopng the cavity floor, 40 elements alongn the arch and 16 elements near every corner (points B and C in Fig. 7) and 100 elements along the loaded part of the surface. The sharp corners B and C were formed by circular arches of small diameter that equals to $0.1R$. To obtain good accuracy 20-22 iterations (Eq. (26)) were performed. The dependence of the maximum hoop stress in the arch part of the cavity and of the hoop stress at the corner point (B) on the load resultant offset from the geometrical axis of symmetry, for $A/R = L/R = 1$ is shown in the Fig. 7. One can see that the stress on the cavity arch decreases with increasing the distance Δ. On the other hand the "corner" hoop

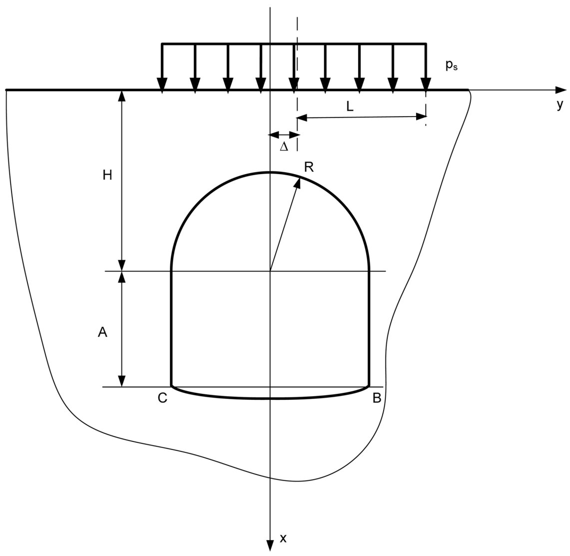

Fig. 6 Horseshoe cavity

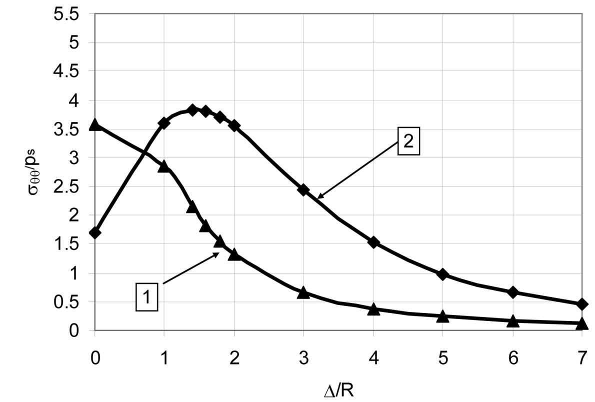

Fig. 7 $A/R = L/R = 1$: 1 (▲) – maximum hoop stress on the arch; 2 (◆) – the stress in the "corner" point B

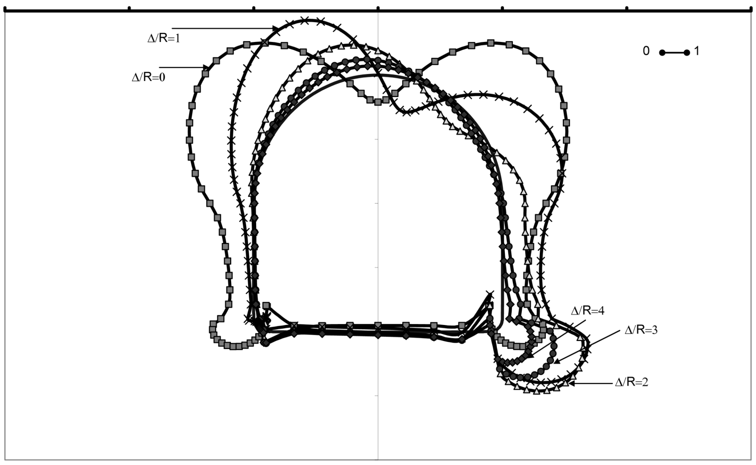

Fig. 8 Hoop stress distribution for $A/R = L/R = 1$

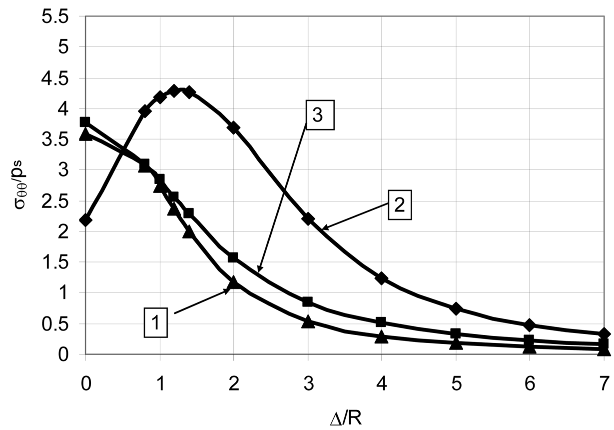

Fig. 9 $A/R = 0.5$, $L/R = 1$: 1 (▲) – maximum hoop stress on the arch; 2 (◆) – the stress in the "corner" point B; 3 (■) - maximum hoop stress on the "equivalent" circle cavity

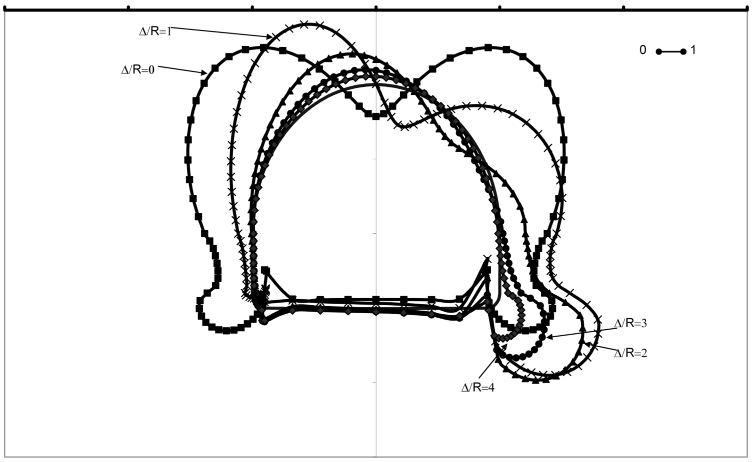

Fig. 10 Hoop stress distribution for $A/R = 0.5$, $L/R = 1$

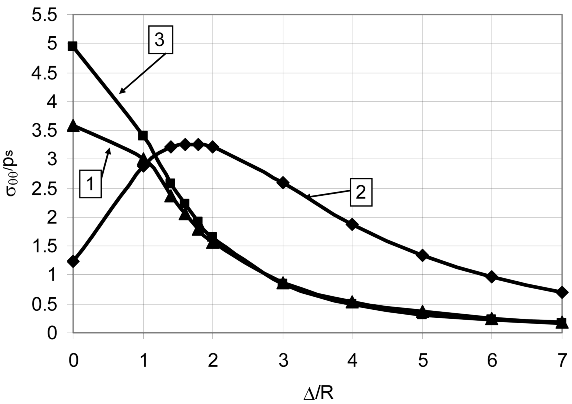

Fig. 11 $A/R = 2$, $L/R = 1$: 1 (▲) – maximum hoop stress on the arch; 2 (◆) – the stress in the "corner" point B; 3 (■) - maximum hoop stress on the "equivalent" circle cavity

stress initially increases to a certain maximum value (in this case it occurs when $\Delta/R \approx 1.3$). For this example the arch and the corner maximum hoop stresses are approximately equal. Examples of stress distributions for various values of Δ are shown in Fig. 8.

When the cavity height A/R is relatively small, the maximum stress at the corner is larger than the maximum stress on the roof arch. Fig. 9 shows the dependence of the maximum hoop stress on the arch and the hoop stress at the corner point (B) for $A/R = 0.5$ and $L/R = 1$. The maximum stress at the corner (the maximum of line 2) is larger than the maximum stress in the arch (the maximum of line 1) by about 20%. Line 3 in Fig. 9 denotes the maximum hoop stress for a circular cavity circumscribing around the examined opening (and may be referred to as an "equivalent circle cavity"). One can see that in the present example the maximum stress on the equivalent circle cavity is closed to the maximum stress on the opening's roof arch. The normalized hoop stress distribution along the cavity for the above example is shown in Fig. 10.

Fig. 11 shows the dependence of the maximum hoop stress in the arch part of the cavity (line 1), the hoop stress at the corner point B (line 2) and the maximum hoop stress on the equivalent

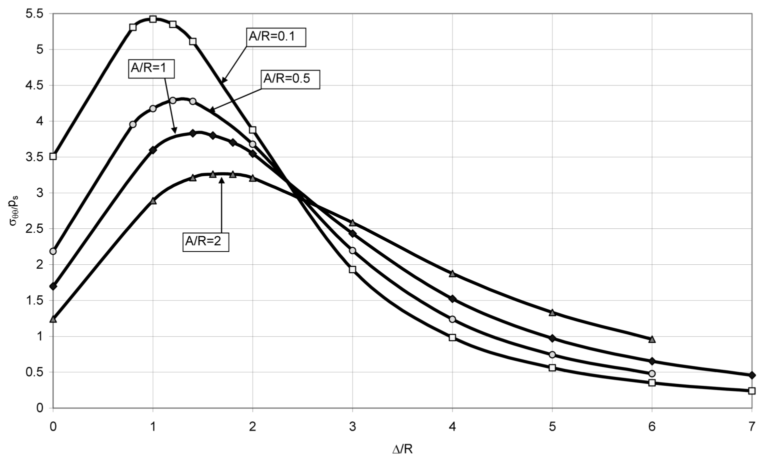

Fig. 12 Corner hoop stresses for various structure heights

circular cavity (line 3) for $A/R = 2$ and $L/R = 1$. In this case the maximum stress at B ($\Delta/R = 1.5$) is smaller than the maximum stress on the arch ($\Delta = 0$) by about 6%. Note that the maximum stress on the equivalent circle cavity significantly exceeds the maximum stress on the horseshoe cavity (by about 36%) and therefore the horseshoe cavity is preferable.

From this example one can conclude that increasing the cavity height (relatively to the roof radius) to some degree (about $A/R = 1$) leads to decrease of the maximum stress at the corners. Further increase is meaningless because the maximum stress is located on the roof arch (and is obtained for the symmetrical load) and this stress slightly increases with A/R.

The hoop stresses at corner B (normalized with the surface pressure) for various opening heights are shown in Fig. 12. One can see that when the height decreases the maximum stress increases and it occurs at a smaller Δ. In all the calculations the maximum stress was found to develop between $\Delta/R = 1$ (the surface loading resultant is located above the corner B) and $\Delta/R = 2$ (the surface loading left edge is located above the corner B).

When the relative loading length L/R along the surface increases, then both stresses (at the corner

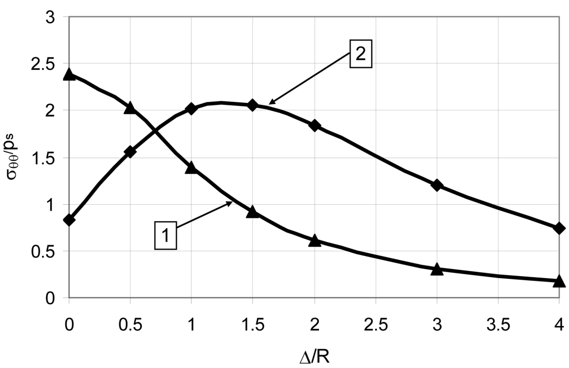

Fig. 13 $A/R = 1$, $L/R = 0.5$: 1 (▲) – maximum hoop stress on the arch; 2 (◆) – the stress in the "corner" point B

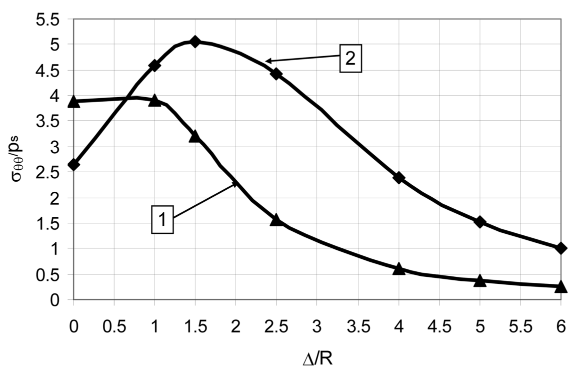

Fig. 14 $A/R = 1$, $L/R = 2$: 1 (▲) – maximum hoop stress on the arch; 2 (◆) – the stress in the "corner" point B

B and the maximum value on the roof region) increase as well, but the rate of the corner stress increase is larger. Thus, if for $L/R = 0.5$ (the height $A/R = 1$) (see Fig. 13) the maximum stress in the roof region is larger than the at the corner (by about 10%) For $L/R = 2$ (see Fig. 14) the stress at the corner exceeds the maximum stress at the roof (by about 20%). As it was shown earlier the stresses are approximately equal when $A/R = L/R = 1$ (Fig. 7).

Figs. 13, 14 show that when a wide area is loaded ($L/R = 2$) the stress at the corner is sensitive to any change of Δ (similar to the case of $L/R = 0.5$), but the maximum stress at the roof region is insensitive to moderate changes in Δ (opposed to the case of $L/R = 0.5$). The normalized hoop stress distribution for such wide surface loading ($L/R = 2$) is shown in Fig. 15. One can see that in the case of a symmetrical loading ($\Delta = 0$) of this length the tensile stress at the top of the structure is very small opposed to the case of a relatively narrow loading (Figs. 8, 10).

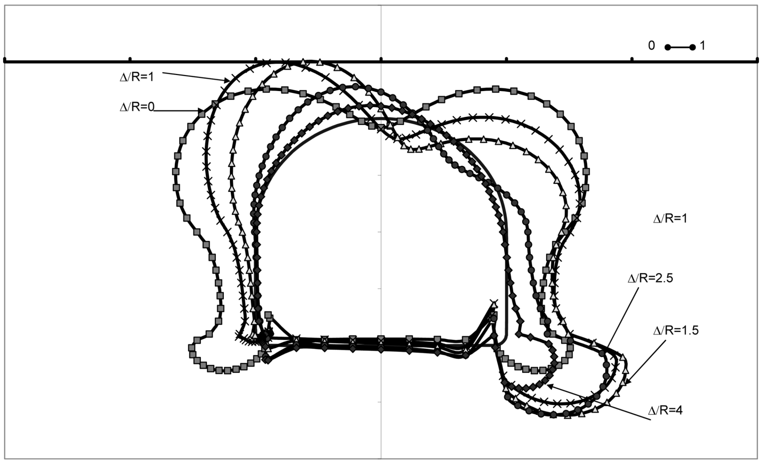

Fig. 15 Hoop stress distribution for $A/R = 1$, $L/R = 2$

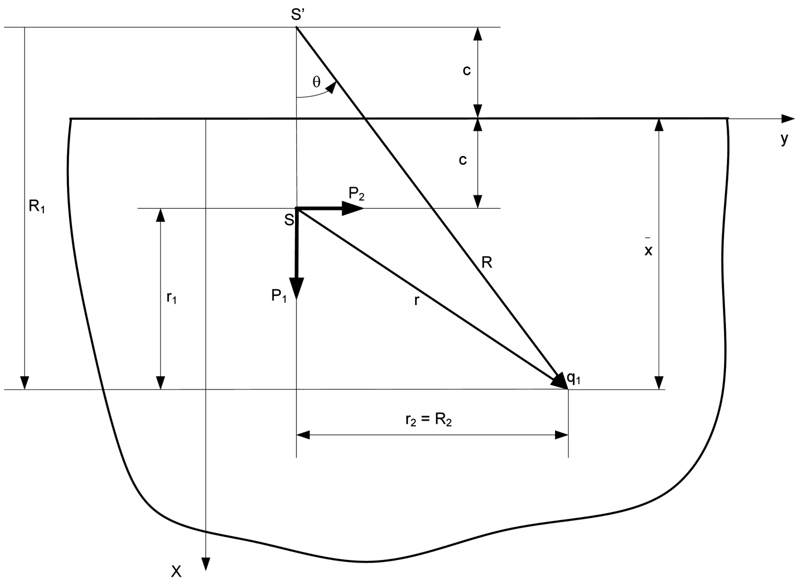

Fig. 16 2D problem

8. Conclusions

The paper develops the application of the BIE method coupled with the Neumann's series for the analysis of an underground unlined tunnel with sharp corners (horseshoe's shape cavity), that is subjected to non-symmetrical surface loading. The special recurrent relationships for half plane were proven assuming that the cavity boundary does not intersect with the boundary of the half plane. To accelerate the series convergence the modified Shanks transform was proposed.

To examine the present approach the hoop stress distribution along the circular opening located in the half plane and subjected to a surface non-symmetrical loading was examined. In the case of a symmetrical loading distribution good correspondence with known analytical results was obtained. It was shown that the maximum stress decreases with increasing asymmetry of the applied load (increasing Δ).

In the case of a horseshoe cavity two points of extreme stresses were identified: a point on the cavity roof (the location depends on the location of the resultant surface pressure) and a point at the corner zone. When the surface load has a symmetrical distribution the maximum hoop stress occurs in the roof area. When the surface pressure resultant is eccentric to the cavity geometrical axis of symmetry the maximum hoop stress in the roof region decreases but the hoop stress variation with Δ at the corner has a convex shape with a maximum magnitude at a certain distance. The eccentricity of the surface pressure that yields the maximum corner stress depends on the opening height and on the segment length of the applied pressure. It was shown also that the absolute maximum (for all the surface load locations) is obtained in the roof when the opening is relatively high or when the pressure acts over a relatively narrow segment. When the opening height is relatively small or when the surface pressure acts over a relatively wide segment (relative to the roof arch radius) the absolute maximum hoop stress is developed at the corner point. The special geometry for which both local maxima are of the same magnitude may be of interest for design purposes and was therefore examined in this analysis. This case is obtained when the opening's wall height and half the loaded segment length were equal to the roof radius.

For all examined cases it was found that 20 iterations only were sufficient to reach a very good accuracy.

Acknowledgements

This research was funded by the Ministry of National Infrastructure, Earth Sciences Division. The research grant is greatly appreciated.

This work was supported by a joint grant from the Center for Absorption in Science of the Ministry of Immigrant Absorption and the Committee for Planning and Budgeting of the Council for Higher Education under the framework of the KAMEA Program.

References

Andersen, L. and Jones, C.J.C. (2006), "Coupled boundary and finite element analysis of vibration from railway tunnels – a comparison of two- and tree-dimensional models", *J. Sound Vib.*, **293**(3-5), 611-625.

Antes, M.Y., Karinski, Y.S. and Yankelevsky, D.Z. (2007), "On the BIEM solution for a half space by neumann

series", *Commun. Numer. Meth. Eng.*, **23**(3), 197-211.
Antes, M.Y., Karinski, Y.S. and Yankelevsky, D.Z. (2007), "The modifiened shanks transform for the solution of elastic problems by Boundary Integral Equation (BIE) method", *Communications in Numerical Methods in Engineering*, (in press)
Antonio, J. and Tadeu, A. (2002), "3D seismic response of a limited valley via bem using 2.5D analytical green's function for an infinite free-rigid layer", *Soil Dyn. Earthq. Eng.*, **22**(8), 659-673.
Brebbia, C.A. and Walker, S. (1980), The Boundary Element Techniques in Engineering. London: Newnes-Butterworths.
Bulichov, N.S. (1989), *Mechanics of Buried Structures*. Moscow.
Cavalcanti, M.C. and Telles, J.C.F. (2003), "Biot's consolidation theory – application of bem with time independent fundamental solution for poro-elastic saturated media", *Eng. Anal. Bound. Elem.*, **27**(2), 145-157.
Chen, Y.Z. (1994), "Multiply circular hole problem for an elastic half-plane", *Comput. Struct.*, **52**(6), 1277-1281.
Cruse, T.A. (1973), "Application of boundary integral equation method to three-dimensional stress analysis", *Comput. Struct.*, **3**, 509-527.
Dajapakse, R.K.N. and Senjuntichi, T. (1995), "Dynamic response of a multi-layered poroelastic medium", *J. Earthq. Eng. Struct. Dyn.*, **24**, 703-722.
Fernando, N.S.M. and Carter, J.P. (1998), "Elastic analysis of buried pipes under surface patch loadings", *J. Geotech. Geoenviron. Eng.,* **124**(9), 720-728.
Fernando, N.S.M., Small, J.S. and Carter, J.P. (1996), "Elastic analysis of buried structures subject to three-dimensional surface loadings", *Int. J. Numer. Anal. Meth. Geotmech,* **20**, 331-349.
Guzina, B.B., Fata, S.N. and Bonnet, M. (2003), "On the stress-wave imaging of cavities in a semi-infinite solid", *Int. J. Solids Struct.*, **40**(6), 1505-1523.
Hatzor, Y.H., Talesnick, M. and Tsesarsky, M. (2002), "Continuous and discontinuous analysis of the bell-shaped caverns at bet guvrin", *Israel. Int. J. Rock Mech. Mining Sci.*, **39**(7), 867-886.
Hurty, W.C. and Rubinstein, M.F. (1964), *Dynamics of Structures*, London: Prentice-Hall.
Kantorovich, L.V. (1958), *Approximate Methods of Higher Analysis*. NY: Interscience.
Karal, F.C. and Keller, J.B. (1964), "Elastic, electromagnetic and other waves in random medium", *J. Math. Phy.*, **3**(4), 537-547.
Karinski, Y.S., Dancygier, A.N. and Leviathan, I. (2003), "An analytical model to predict static contact pressure on a buried structure", *Eng. Struct.*, **25**(1), 91-101.
Karinski, Y.S., Shershnev, V.V. and Yankelevsky, D.Z. (2004), "The effect of an interface boundary layer on the resonance properties of a buried structure", *Earthq. Eng. Struct. Dyn.*, **33**(2), 227-247.
Karinski, Y.S., Shershnev, V.V. and Yankelevsky, D.Z. (2007), "Analytical solution of the harmonic waves diffraction by a cylindrical lined cavity in poroelastic saturated medium", *Int. J. Numer. Anal. Meth. Geomech.* (in press)
Kim, M.K., Lim, Y.M. and Rhee, J.W. (2000), "Dynamic analysis of layered half planes by coupled finite and boundary elelments", *Eng. Struct*., **22**, 670-680.
Kumar, P. (1985), "Static Infinite Element Formulation", *J. Struct. Eng.*, **111**(11), 2355-2372.
Kupradze, V.D., Gegelia, T.G., Baseleisvili, M.O. and Burculadze, T.V. (1979), Three-Dimentional Problems of Theory of Elasticity and Thermoelasticity. Amsterdam, NY, Oxsford: North-Holland Series in Applied Math. and Mech., **25**, 1-929.
Manolis, G.D. (2003), "Elastic wave scattering around cavities in inhomogeneous continua by the BEM", *J. Sound Vib.*, **266**(2), 281-305.
Melan, E. (1932), "Der Spannungszustand der Durch Eine Einzelcraft im Innert Deanspruchten Halbscheibe", *Z. Angew. Math. Mech*., **12**, 343-346.
Mikhlin, S.G. (1965), *Multidimensional Singular Integrals and Integral Equations*. Oxford: Pergamon.
Moore, I.D. (1987), "Response of buried cylinders to surface loads", *J. Geotech. Eng*., **113**(7), 758-773.
Moore, I.D. and Branchman, R.W. (1994), "Three-dimensional analysis of flexible circular culverts", *J. Geot. Eng.*, **120**(10), 1829-1844.
Moser, A.P. (2001), *Buried Pipe Design*. McGraw-Hill.
Parton, V.Z. and Perlin, P.I. (1984), "Mathematical methods of the theory of elasticity", Parts 1,2. Moscow: MIR.
Rogier-Hendrik, De-Zutter D. (2002), "A fast technique based on perfectly matched layers to model

electromagnetic from wires embedded in substrates", *Radio Science*, **37**(2), 101-106.

Schnack, E. and Tuerke, K. (1997), "Domain decomposition with BEM and FEM", *Int. J. Numer. Meth. Eng.*, **40**(14), 2593-2610.

Shanks, D. (1955), "Non linear transformation of divergent and slowly convergent series", *Math. Phys.*, **34**, 1-42.

Small, J.C. and Wang, H.K.W. (1988), The use of integral transforms in solving three-dimensional problems in geomechanics", *Comput. Geotech.*, **6**, 199-216.

Surjadinata, J., Hull, T.S., Carter, J.P. and Poulos, H.G. (2006), "Combined finite- and boundary-element analysis of the effects of tunneling on single piles", *Int. J. Geomech.*, **6**(5), 374-377.

Szechny, K. (1973), *The Art of Tunneling*. Budapest.

Talles, J.C.F. (1983), *The Boundary Element Method Applied to Inelastic Problems*. Springer.

Appendix A (see Fig. 16)

- The additional terms of the Green tensor:

$$u^c_{11} = K_d\left\{\{-[8(1-\nu)^2-(3-4\nu)]\ln R + \frac{(3-4\nu)R_1^2-2c\bar{x}}{R^2} + \frac{4c\bar{x}R_1^2}{R^4}\right\}$$

$$u^c_{12} = K_d\left\{\frac{(3-4\nu)r_1r_2}{R^2} + \frac{4c\bar{x}R_1r_2}{R^4} - 4(1-\nu)(1-2\nu)\theta\}\right\}$$

$$u^c_{21} = K_d\left\{\frac{(3-4\nu)r_1r_2}{R^2} - \frac{4c\bar{x}R_1r_2}{R^4} + 4(1-\nu)(1-2\nu)\theta\}\right\}$$

$$u^c_{22} = K_d\left\{-[8(1-\nu)^2-(3-4\nu)]\ln R + \frac{(3-4\nu)r_2^2+2c\bar{x}}{R^2} - \frac{4c\bar{x}r_2^2}{R^4}\right\}$$

$$\sigma^c_{111} = -K_s\left\{\frac{(3\bar{x}+c)(1-2\nu)}{R^2} + \frac{2R_1(R_1^2+2c\bar{x})-4\bar{x}r_2^2(1-2\nu)}{R^4} - \frac{16c\bar{x}R_1r_2^2}{R^6}\right\}$$

where $\theta = arctan\left(\frac{R_2}{R_1}\right)$; $K_d = \frac{1}{8\pi(1-\nu)G}$

- The additional terms of the stress operator:

$$\sigma^c_{121} = -K_sr_2\left\{-\frac{1-2\nu}{R^2} + \frac{2[\bar{x}^2-2c\bar{x}-c^2+2\bar{x}R_1(1-2\nu)]}{R^4} + \frac{16c\bar{x}R_1^2}{R^6}\right\}$$

$$\sigma^c_{221} = -K_s\left\{\frac{(\bar{x}+3c)(1-2\nu)}{R^2} + \frac{2[R_1(r_2^2+2c^2)-2cr_2^2+2\bar{x}r_2^2(1-2\nu)]}{R^4} + \frac{16c\bar{x}R_1r_2^2}{R^6}\right\}$$

$$\sigma^c_{112} = -K_sr_2\left\{-\frac{1-2\nu}{R^2} - \frac{2[c^2-\bar{x}^2+6c\bar{x}-2\bar{x}R_1(1-2\nu)]}{R^4} + \frac{16c\bar{x}r_2^2}{R^6}\right\}$$

$$\sigma^c_{122} = -K_s\left\{\frac{(3\bar{x}+c)(1-2\nu)}{R^2} + \frac{2[(2c\bar{x}+r_2^2)R_1-2\bar{x}R_1^2(1-2\nu)]}{R^4} - \frac{16c\bar{x}R_1r_2^2}{R^6}\right\}$$

$$\sigma^c_{222} = -K_sr_2\left\{\frac{3(1-2\nu)}{R^2} + \frac{2[r_2^2-4c\bar{x}-2c^2-2\bar{x}R_1(1-2\nu)]}{R^4} + \frac{16c\bar{x}R_1^2}{R^6}\right\}$$

$\sigma^c_{211} = \sigma^c_{121}$; $\sigma^c_{212} = \sigma^c_{122}$, where: $K_s = \frac{1}{4\pi(1-\nu)}$